

Article

CO Tolerance and Stability of Graphene and N-Doped Graphene Supported Pt Anode Electrocatalysts for Polymer Electrolyte Membrane Fuel Cells

Martin González-Hernández ¹, Ermete Antolini ²  and Joelma Perez ^{1,*}¹ São Carlos Institute of Chemistry, University of São Paulo, São Paulo 13560-970, Brazil; caromanto@hotmail.com² Scuola di Scienza dei Materiali, Via 25 aprile 22, Cogoleto, 16016 Genova, Italy; ermantol@libero.it

* Correspondence: jperez@iqsc.usp.br; Tel.: +55-1633739926

Received: 24 April 2020; Accepted: 25 May 2020; Published: 27 May 2020



Abstract: Pt electrocatalysts supported on pristine graphene nanosheets (GNS) and nitrogen-doped graphene nanoplatelets (N-GNP) were prepared through the ethylene glycol process, and a comparison of their CO tolerance and stability as anode materials in polymer electrolyte membrane fuel cells (PEMFCs) with those of the conventional carbon (C)-supported Pt was made. Repetitive potential cycling in a half cell showed that Pt/GNS catalysts have the highest stability, in terms of the highest sintering resistance (lowest particle growth) and the lowest electrochemically active surface area loss. By tests in PEMFCs, the Pt/N-GNP catalyst showed the highest CO tolerance, while the poisoning resistance of Pt/GNS was lower than that of Pt/C. The higher CO tolerance of Pt/N-GNP than that of Pt/GNS was ascribed to the presence of a defect in graphene, generated by N-doping, decreasing CO adsorption energy.

Keywords: PEMFC; CO tolerance; stability; platinum; N-doped graphene nanoplatelets

1. Introduction

Pt/C is widely used as an anode material in H₂-fueled polymer electrolyte membrane fuel cells (PEMFCs). Since H₂ is commonly obtained by hydrocarbon reforming, it follows that CO is present as a contaminant, which is adsorbed on Pt active sites, reducing fuel cell performance [1]. To increase CO tolerance, Pt-based electrocatalysts, especially Pt-Ru and Pt-Mo, are a hopeful solution [1–5].

A major hindrance regarding the utilization of carbon-supported platinum is the poor resistance of carbon surface to be oxidized, resulting in Pt surface area loss, owing to both Pt coalescence and Pt way out from the carbon support [6–8]. Moreover, carbon black has no effect on CO tolerance of Pt. Thus, materials other than carbon black that improve CO tolerance of Pt and with higher structural stability and higher resistance to carbon surface oxidation were investigated as Pt supports [9–12]. Tests in fuel cells indicated that graphene nanosheets (GNS) are a suitable PEMFC catalyst support [12]. Especially, nitrogen-doped graphene proved promising for their use in PEMFCs [13,14].

The stability of Pt supported on N-functionalized-graphene was assessed by different theoretical works [15–19]. By density functional theory (DFT) analysis it was found that graphene N-doping improves the binding energy of platinum to the substrate: the binding energy increased by two-fold, resulting in an enhancement of platinum stability [15]. N-doping gives rise to the formation of localized defects near to the Fermi level of graphene, stabilizing Pt atoms. Nitrogen atoms presence into carbon lattice gives rise to three main kinds of nitrogen functional groups, namely, pyridinic N, pyrrolic N, and graphitic N species [16]. Among these N species, the more effective at binding Pt are pyridinic N and pyrrolic N species [17,18].

DFT analysis showed that ripening of Pt particle supported on highly oriented pyrolytic graphite (HOPG) with agglomerated vacancies is highly energetically favorable, while ripening Pt particles on HOPG with pyridinic N and pyrrolic N is hindered [18]. The theoretical higher stability of N-doped graphene than pristine graphene was confirmed by experimental results [20]: the retention of the electrochemically active surface area (ECSA) following repetitive potential cycling of N-doped reduced graphene oxide was higher than that of undoped reduced graphene oxide.

Moreover, theoretical works showed that nitrogen doping in graphene enhances CO tolerance of Pt nanoparticles [21–24]. First, by DFT calculations Tang et al. [21] compared the CO oxidation on Pt single atoms on pristine and defective graphene: unlike CO oxidation on Pt/pristine-graphene, the Pt/defective-graphene showed high activity for CO oxidation. Defects can be introduced in graphene by N-doping. Kim et al. [22] observed that the binding energy of Pt nanoparticles on N defects is about three times larger than on pristine graphene. They found that the adsorption energy ϵ_{ad} of H₂ and CO on Pt nanoparticles are not correlated, but the difference in ϵ_{ad} between H₂ and CO, $\Delta\epsilon_{ad} = (\epsilon_{CO} - \epsilon_{H_2})$, is relatively well correlated to the average energy of *d* electrons (*d*-band center) of surface Pt atoms (ϵ_{dc}) of Pt clusters. As low is $\Delta\epsilon_{ad}$ between CO and H₂, as high is CO tolerance. Because CO has stronger electron affinity than H₂, which indicates a larger amount of electron back donation from Pt, CO adsorption is more sensitive to the Pt *d*-band profile than H₂ adsorption. The strong binding of Pt to N-doped graphene lowers ϵ_{dc} and thus reduces ΔE_{ad} . Regarding the role of N configurations, it was found that the activation barrier for the O₂ adsorption is much higher on both the pyridinic nitrogen site and the nearest carbon atom than on graphitic nitrogen sites, while pyridinic nitrogen weakens the O–O bond [23]. Both the reaction thermodynamics and kinetics suggest that CO oxidation over PtN₃ would proceed through the Langmuir–Hinshelwood mechanism [19].

Various experimental works were addressed to the evaluation of CO tolerance of graphene or N-doped graphene-supported catalysts either directly during H₂ oxidation in the presence of CO [25–27], or indirectly during methanol oxidation (CO as an intermediate species formed during the methanol oxidation reaction) [28–32]. Hydrogen oxidation in the presence of CO was carried out only on one type of graphene as the catalyst support, either pristine [25,26] or N-doped [27], and the positive effect of graphene on CO tolerance was ascribed to the formation of sub-nano Pt particles in pristine graphene-supported Pt or to the presence of N groups in N-doped graphene-supported Pt. Conversely, the poisoning tolerance during the methanol oxidation of Pt supported on pristine and N-doped graphene was compared in different works [28–32]: the ratio of the forward anodic peak current (I_f) to the reverse anodic peak current (I_b) is commonly used to evaluate the catalyst tolerance toward the intermediate poisoning carbonaceous species (particularly CO but also other oxygenated species). A higher ratio of I_f/I_b indicates the less accumulation of poisoning species on the Pt nanoparticles, suggesting better CO tolerance. A higher poisoning tolerance during methanol oxidation of Pt-supported N-doped graphene than that of Pt-supported pristine graphene was observed by Cogenly and Yurtcan [28], Liu et al. [29], and Tao et al. [30], whereas circa the same and a lower poisoning tolerance of Pt/N-GNS than that of Pt/GNS was observed by Ma et al. [31] and Xin et al. [32], respectively.

The majority of previous works dealing on the problem of the poisoning of the Pt/C anode catalyst in PEMFCs by the CO presence in the fuel were addressed to the effect of the addition of a second metal to Pt on CO tolerance [1,4]. CO desorption is facilitated by the second metal, either through the electronic effect or the bifunctional mechanism. A modification of the electronic structure of Pt by alloying with a transition metal reduces the CO adsorption energy and favors the H₂ adsorption on Pt active sites. According to the bifunctional mechanism, the second metal is able to activate H₂O at low potentials than Pt, facilitating the oxidation of adsorbed CO by supplying oxygen atoms at an adjacent site. In this work, instead, we evaluated the effect of the support on CO tolerance of pure Pt. For the first time an experimental comparison of the CO tolerance of pristine and N-doped graphene was carried out. Thus, to assess the influence of N-doping

on the CO tolerance of Pt supported on both on pristine and N-functionalized graphene, we prepared GNS and nitrogen-doped graphene nanoplatelets (N-GNPs)-supported Pt catalysts, and compared the performance of PEMFCs with these anode catalysts in the presence and in the absence of CO with each other and with that of a PEMFC with conventional Pt/C.

2. Results

2.1. Physical Characterization

The EDX composition of the Pt/GNS, Pt/N-GNP, and Pt/C electrocatalysts is shown in Table 1: the metal content of all the catalysts was in a very good agreement with the nominal composition (20 wt % Pt). To evaluate the Pt content and the thermal stability, a thermogravimetric analysis (TGA) was carried out on all the catalysts. TGA curves of Pt/GNS, Pt/N-GNP, and Pt/C catalysts are shown in Figure 1. As reported by Avcioglu et al. [33] for Pt/C, these curves can be separated into three regions with increasing temperature. The first region is related to the removal of water and volatile species. The second region, where a remarkable weight loss takes place, is related to Pt catalyzed carbon oxidation. The third region, doesn't present weight loss, and the constant weight represents the amount of Pt. In the absence of platinum, carbon black and graphene have similar thermal stability [34]. In Pt presence the carbon oxidation occurs at lower temperatures.

Table 1. Pt mass by Dispersive Energy (EDX) and thermogravimetric analysis (TGA) measurements, Pt lattice parameter and crystallite size by XRD analysis, and Pt particle size by Transmission Electronic Microscopy (TEM) micrographs of Pt/C, Pt/GNS, and Pt/N-GNP (d_n : number averaged particle size and d_G : average Gaussian Pt particle size).

Catalyst	Pt Mass (EDX)/%	Pt Mass (TGA)/%	Lattice Parameter/nm	Crystallite Size (XRD)/nm	Particle Size (TEM)/nm			
					As-Prepared	Cycled	d_n	d_G
Pt/C	20.0	17.5	0.3888	2.2	1.9 ± 0.2	1.9	3.6 ± 1.2	2.8
Pt/GNS	18.6	19.4	0.3913	1.9	2.3 ± 0.4	2.0	3.4 ± 1.7	3.3
Pt/N-GNP	21.6	23.1	0.3916	3.1	2.3 ± 0.2	2.3	4.0 ± 1.1	3.9

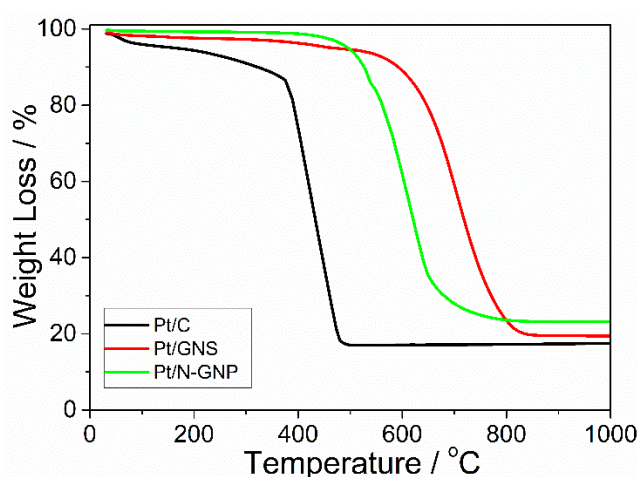


Figure 1. Thermogravimetric analyses of Pt/C, Pt/GNS and Pt/N-GNP catalysts. The measurements were performed in air atmosphere up to 1000 °C with a heating ramp of 10 °C min⁻¹. Abbreviations: GNS, graphene nanosheets; GNP, graphene nanoplatelets.

For Pt/GNs, the carbon oxidation occurred between 555 and 840 °C, at higher temperatures than Pt/C (between 370 and 485 °C), in agreement with the results of Chiang et al. [34]: the deposition of Pt nanoparticles on GNS slightly decreased its resistance to oxidation, but the deposition of Pt nanoparticles on the Vulcan carbon significantly decreased its resistance to oxidation. The functionalization of graphene decreases its thermal stability, thus the carbon oxidation in the presence of Pt lies between that of carbon black and that of pristine graphene. As can be seen in Table 1, the Pt content in the catalysts by TGA measurements was in an acceptable agreement with that obtained by EDX analysis.

The XRD patterns of the Pt/GNS, Pt/N-GNP, and Pt/C electrocatalysts are shown in Figure 2. All the patterns show the characteristic peaks of the face centered cubic (fcc) crystalline Pt. In addition, the large sharp peak at 26° and the smaller peaks at 2θ values around 44.5°, 54.5°, 77°, and 83.5° in Pt/GNS and Pt/N-GNP are related to the (002), (10), (004), (11), and (006) reflexions of nanographene [35,36]. The first broad peak of catalysts at a 2θ value of around 25° is ascribed to carbon support. The values of the lattice parameter (*a*) are reported in Table 1. The lattice parameter of Pt/C was lower than that of Pt/GNS, Pt/N-GNP as it decreases nonlinearly with decreasing the particle size [37]. The average crystallite sizes of the Pt/GNS, Pt/N-GNP, and Pt/C electrocatalysts were evaluated using Scherrer's equation (see Table 1).

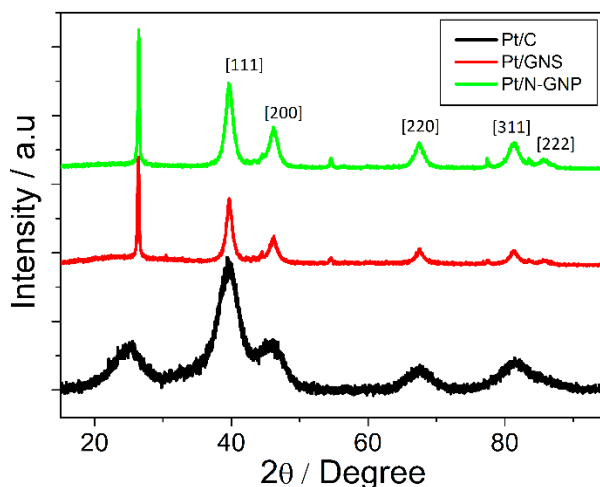


Figure 2. The X-ray diffraction technique (XRD) patterns of Pt/C, Pt/GNS, and Pt/N-GNP catalysts.

To determine the oxidation states of Pt, XPS (X-ray Photon Spectroscopy) analysis was carried out on the Pt/GNS, Pt/N-GNP, and Pt/C electrocatalysts. The XPS patterns of the Pt 4*f* region are shown in Figure 3a. The Pt 4*f* XPS signals have two peaks corresponding to the 4*f*_{5/2} and 4*f*_{7/2} states, which have been deconvoluted into three different Pt oxidation states (Pt⁰, Pt²⁺, and Pt⁴⁺ oxidation states), the percentage of Pt oxidation states in the different catalysts is shown in Table 2. The amount of platinum metal (Pt⁰) in graphene and N-doped graphene-supported Pt was higher than that in carbon black-supported Pt. Moreover, XPS measurements were carried out to analyze the N configurations in nitrogen-doped graphene. The XPS pattern of the N 1*s* region of the Pt/N-GNP electrocatalyst is shown in Figure 3b.

The presence of nitrogen atoms into carbon lattice gives rise to three main kinds of nitrogen functional groups, that are pyridinic N, pyrrolic N, and graphitic (quaternary) N species [16]. The N1*s* spectrum can be de-convoluted to three individual peaks, which represent three nitrogen configurations within carbon structures, Figure 3. The binding energy centered at ca. 398.3 eV, 399.8 eV, and 401.8 eV can be assigned to the pyridinic N, pyrrolic N, and graphitic N, respectively. The relative amount of the N configurations is reported in Table 2. The N/C value by XPS measurements was 0.007.

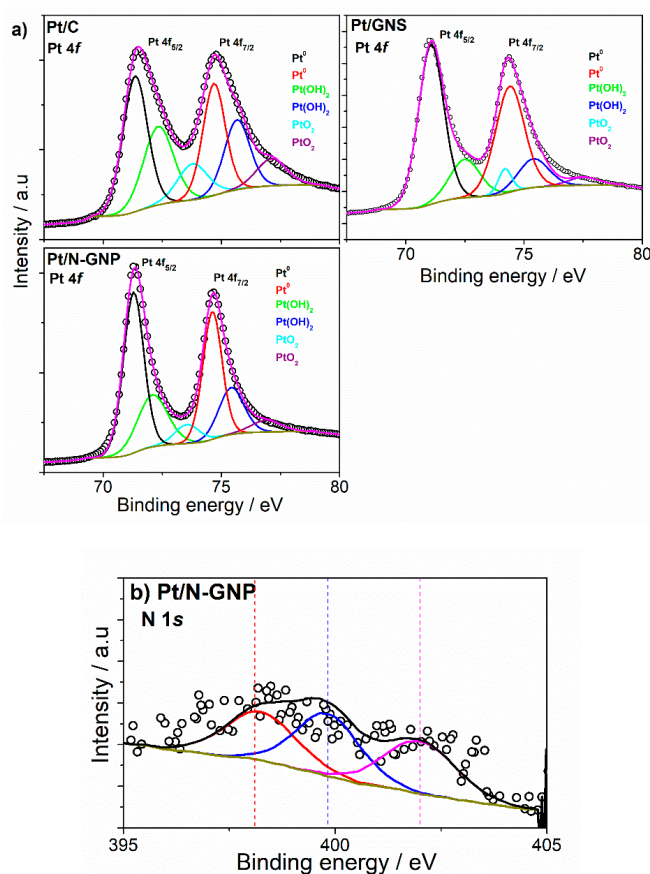


Figure 3. XPS (X-ray Photon Spectroscopy) spectra of (a) Pt 4f of Pt/C, Pt/GNS, and Pt/N-GNP catalysts and (b) Pt/N-GNP N 1s.

Table 2. Amount of Pt 4f and N 1s oxidation states (at %) in Pt/C, Pt/GNS, and Pt/N-GNP by XPS analysis.

Catalyst	Pt 4f _{7/2}			N 1s		
	Pt ⁰	Pt ²⁺	Pt ⁴⁺	Pyridinic	Pyrrolic	Graphitic
Pt/C	49.21	34.80	15.99	-	-	-
Pt/GNS	63.96	26.14	9.89	-	-	-
Pt/N-GNP	60.79	30.78	8.43	31.0	35.5	33.5

Figure 4a–c reports TEM images and the histograms of the particle size distribution of the as-prepared Pt/C, Pt/GNS, and Pt/N-GNP electrocatalysts. As shown in Figure 4, Pt particles are homogeneously placed on the support, with small agglomeration on Pt/GNS and Pt/N-GN. The histograms of Pt/C and Pt/N-GN particle size are well represented by Gaussian fitting. Conversely, the particle size histogram of the Pt/GNS catalyst showed a slightly asymmetrical distribution, with a tail in the larger particle size region. As shown in Figure 4d–f, following RPC (Repetitive potential cycling) an increase in the particle size and a wider particle size distribution can be observed for all the catalysts. After cycling, the particle size histograms of Pt/GNS and Pt/N-GN are well represented by a Gaussian fitting, while the particle size histogram of the Pt/C goes from a symmetrical to an asymmetrical distribution, with a tail in the larger particle size region. The values of the average Gaussian Pt particle size (d_G) of Pt/GNS, Pt/N-GNP, and Pt/C are reported in Table 1. The number averaged particle size (d_n) have been calculated using Equation (1):

$$d_n = \frac{\sum_k n_k d_k}{\sum_k n_k} \quad (1)$$

where n_k is the frequency of occurrence of particles with size d_k . The values of d_n are reported in Table 1. The Pt/GNS and Pt/N-GNP present the same value of d_n . The $(d_n^{\text{RPC}} - d_n^0)/d_n^0$ ratio, where d_n^{RPC} and d_n^0 are the particle size after and before cycling, respectively, indicates the sintering resistance of Pt particles, being the sintering resistance as higher as the lower value of the $(d_n^{\text{RPC}} - d_n^0)/d_n^0$ ratio. For Pt/GNS, the value of the $(d_n^{\text{RPC}} - d_n^0)/d_n^0$ ratio (0.48) was the lowest, followed by that of Pt/N-GNP (0.74) and that of Pt/C (0.89). This result does not agree with the theoretical calculations previously reported, reporting higher stability of Pt/N-GNS than Pt/GNS. To support this result there is a work of Naumov et al. [38], which evaluated the stability of nitrogen-doped graphene flakes with theoretical and experimental techniques. They supposed that nitrogen dopants in the graphene sheet interact with H^+ at the electrode–electrolyte interface, leading to NH_3 scission with the formation of vacancies. N loss and vacancy formation make Pt particles prone to ripening. This could explain the lower structural stability of Pt/N-GNP than that of Pt/GNS. Moreover, the low stability of N-GNP could be due to the presence of a too high nitrogen content [39]. The difference between d_G and d_n is an index of the distribution asymmetry. The asymmetry increases with increasing the $A_G = (d_n - d_G)/d_n$ value from 0 to 1. The low value of A_G for Pt/C indicates a uniform particle size distribution. After RPC, the Pt/C catalyst showed a A_G value (0.22) remarkably higher than that Pt/GNS (0.029) and Pt/N-GNP (0.025). Summarizing, the Pt/C catalyst showed a lower structural stability than Pt/GNS and Pt/N-GNP, having a lower sintering resistance and a higher asymmetry than graphene-supported catalysts.

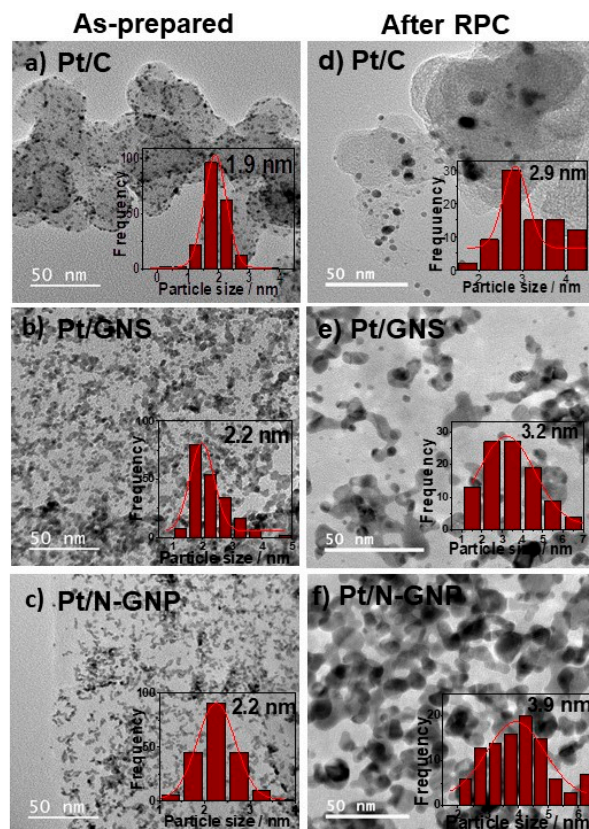


Figure 4. TEM micrographs and histograms of: (a) Pt/C; (b) Pt/GNS, (c) Pt/N-GNP, (d) Pt/C(RPC), (e) Pt/GNS, and (f) Pt/N-GNP(RPC).

2.2. Electrochemical Characterization

CO stripping measurements were carried out to evaluate the catalytic activity for CO oxidation and to determine the electrochemically active surface area (ECSA). The CO oxidation curves of as-prepared and cycled Pt/C, Pt/GNS, and Pt/N-GNP are shown in Figure 5a–c, respectively. The shape of the CO stripping curves before RPC of Pt/GNS and Pt/N-GNP was different than that of Pt/C: the CO stripping curve of Pt/C presented only one peak with a value of the onset potential of 0.69 V vs. RHE and a maximum at ca. 0.76 V vs. RHE, whereas those of Pt/GNS and Pt/N-GNP were characterized by the overlapping of two peaks with the onset potential at 0.58 and 0.35 V vs. RHE, respectively, and two maxima at 0.67 and 0.70 V vs. RHE for Pt/GNS and 0.65 V and 0.68 V vs. RHE for Pt/N-GNP. The different CO peak potential between carbon black-supported Pt and graphene-supported Pt/C has to be ascribed to the different CO binding energy. The change of the electronic structure of some Pt atoms near to N atoms account for multiple CO oxidation peaks. These results indicate a higher ability for CO oxidation of Pt/N-GNP than that of Pt/C. After RPC, for Pt/C a minor peak appeared at lower potential while the main peak shifted to slightly higher potential with reduced intensity, whereas the CO stripping curves of Pt/GNS and Pt/N-GNP didn't change the shape, but reduced their intensity. The electrochemically active surface areas (ECSAs) of Pt/C, Pt/GNS, and Pt/N-GNP were evaluated from the CO_{ad} oxidation charge (see Table 3).

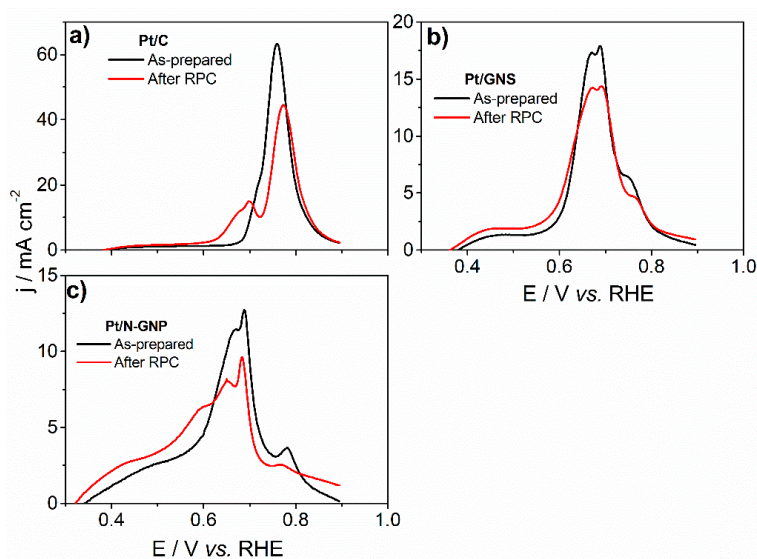


Figure 5. CO oxidation on as-prepared and cycled Pt/C (a), Pt/GNS (b), and Pt/N-GNP (c).

Table 3. Electrochemically active surface area (ECSA) values ECSA loss after RPC of Pt/C, Pt/GNS, and Pt//N-GNP.

Catalyst	ECSA before RPC cm ² g ⁻¹	ECSA after RPC cm ² g ⁻¹	ECSA Loss %
Pt/C	66.0	61.9	6.2
Pt/GNS	32.9	32.2	2.2
Pt//N-GNP	25.4	24.9	1.9

The lower ECSA of Pt/GNS and Pt/N-GNP than that of Pt/C could be partially ascribed to their slightly larger particle size, but perhaps should be attributed to Pt particle agglomeration, in agreement with TEM analysis. The same result, that is, a similar particle size but a lower ECSA

for graphene-based-supported Pt than carbon black-supported Pt, was observed by Arteaga et al. [40], and was ascribed to Pt agglomeration. After ageing test, a decrease of the ECSA was observed, owing to particle growth and Pt loss. The decrease of the ECSA, however, was lower than that expected on the basis of the degree of particle growth, likely due to a counteracting cleaning effect by RPC. The ECSA loss of Pt/GNS and Pt/N-GNP following RPC was lower than that of Pt/C (Figure 5 and Table 3), indicating a higher stability of graphene and N-graphene-supported catalysts.

Polarization measurements of PEMFCs with H₂ and H₂ containing 100 ppm CO, with Pt/C, Pt/GNS and Pt/N-GNP were carried out, as shown in Figure 6a. in the presence of CO the performance of all the cells decreased, owing to CO adsorption on Pt sites, hindering H₂ adsorption. The PEMFC performance, without CO, depends little on the type of support for current densities up to 0.5 mA cm⁻², in the order Pt/C > Pt/N-GNP > Pt/GNS. At higher current densities a lower performance of the cells with graphene and N-graphene-supported catalysts is observed, due to the lower ECSA. The higher performance of the cell with Pt/N-GNP than that with Pt/GNS both at low and high current densities is due to a positive effect of nitrogen presence on the hydrogen oxidation, as reported by Chadran et al. [41]. In the presence of CO, instead, the cell with Pt/N-GNP showed a better performance than that of the cells with Pt/C and Pt/GNS, resulting from the superior CO tolerance of the N-GNP support. In the absence of graphene functionalization and subnano Pt particles, the CO tolerance of graphene-supported Pt was lower than that of Pt/C. The order of the performance at 0.5 mA cm⁻² was Pt/N-GNP > Pt/C > Pt/GNS (Figure 7).

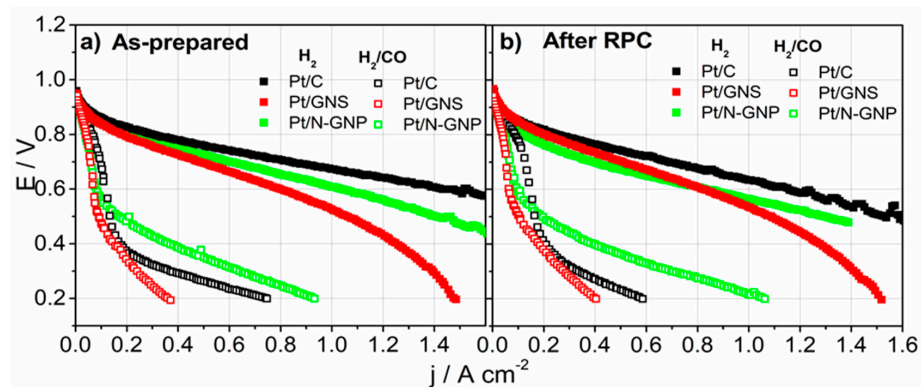


Figure 6. V/j curves of PEMFCs with Pt/C, Pt/GNS, and Pt/N-GNP fed with H₂ (closed symbols) and H₂/100 ppm CO (open symbols) as-prepared (a) and following (b) RPC.

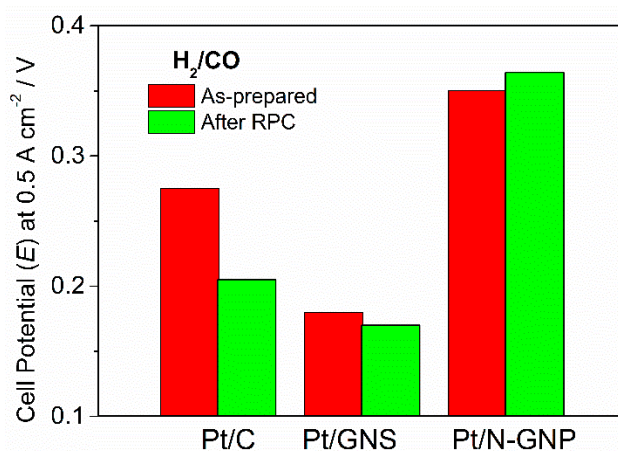


Figure 7. Cell potential at 0.5 A cm⁻² with Pt/C, Pt/GNS, and Pt/N-GNP as anode materials fed with H₂/CO.

This experimental result confirms the theoretical studies, indicating that, unlike CO oxidation on pristine graphene-supported Pt, nitrogen doping in graphene improves CO tolerance of Pt nanoparticles. The hydrogen reactivity can be evaluated by the relative occupation ratio R , that is the ratio of adsorption sites occupied by H_2 to those occupied by CO [22]:

$$R = (\Sigma[e^{(\mu_{H_2} - \epsilon_{H_2})/kT} / (1 + e^{(\mu_{H_2} - \epsilon_{H_2})/kT} + e^{(\mu_{CO} - \epsilon_{CO})/kT})]) / N \quad (2)$$

where μ_{H_2} and μ_{CO} are the chemical potentials and ϵ_{H_2} and ϵ_{CO} are the adsorption energy of hydrogen and carbon monoxide, and N is the number of available adsorption sites. The CO tolerance of Pt nanoparticles increases with increasing R . The higher CO tolerance of Pt/N-GNP than that of Pt/GNS can be explained by the presence of a defect in graphene generated by N-doping.

Defects in N-doped graphene remarkably enhance Pt binding strength (E_b) and lower the average energy of Pt d electrons (d -band center) (ϵ_{dc}) compared to pristine graphene [22]. As previously reported, $\Delta\epsilon_{ad} = (\epsilon_{CO} - \epsilon_{H_2})$ decreases with increasing d -band center of surface Pt atoms (ϵ_{dc}). Due to CO adsorption being more sensitive to the Pt d -band profile than H_2 adsorption, a decrease of $\Delta\epsilon_{ad}$ is mainly due to the decrease of ϵ_{CO} . A decrease of ϵ_{CO} results in an increase of R (see Equation (2)) and, as a consequence an increase of CO tolerance. Moreover, by EIS measurements it was reported that the incorporated nitrogen atoms induced changes at the Fermi level by opening the band gap of graphene and enhancing the charge transfer, and as a consequence lowering the charge-transfer resistance [42]. This could contribute to the improvement of CO tolerance.

To assess the electrochemical stability polarization measurements of PEMFCs, fed with H_2 and H_2/CO , with aged Pt/C, Pt/GNS, and Pt/N-GNP were carried out. In the absence of CO, as for as-prepared catalysts, the performance of PEMFC with Pt/C was higher than that of Pt/GNS and Pt/N-GNS (Figure 6b). Unlike what was observed before RPC, up to 0.9 A cm^{-2} the performance of the cell with Pt/GNS was higher than that with Pt/N-GNP, likely due to the higher structural stability of pristine graphene. For current density $> 0.9 \text{ A cm}^{-2}$, instead, the positive effect of nitrogen presence on the hydrogen oxidation is prevailing, and the performance of the cell with Pt/N-GNP was higher than that with Pt/GNS. As for as-prepared catalysts, for cycled catalysts, in the presence of CO the performance of the cells with aged catalysts was Pt/N-GNP $>$ Pt/C $>$ Pt/GNS (Figures 6b and 7). In the presence of CO, compared to the cell with as-prepared catalysts, after ageing a decrease of the performance of the cell with Pt/C as anode catalyst was observed, due to the ECSA decrease by Pt particle growth, whereas the cell with for Pt/GNS and Pt/N-GNP as anode catalyst presented a substantial stability, due to a lower ECSA loss, and, in the case of Pt/N-GNP, to the weaker adsorption of CO on the larger Pt particles [43,44], reducing the poisoning of the catalyst.

The dependence of the anode overpotential η ($\eta = E_{H_2} - E_{H_2/CO}$) on the current density for Pt/C, Pt/GNS, and Pt/N-GNP electrocatalysts before and after RPC is shown in Figure 8. Both before and after RPC, for current densities $> 0.15 \text{ A cm}^{-2}$, the overpotential was in the order Pt/N-GNP $<$ Pt/C $<$ Pt/GNS. Following ageing, a decrease of the overpotential for all the catalysts, in particular for Pt/N-GNP, which presents the largest Pt particle size, can be observed in Figure 8, due to the weaker adsorption of CO on the larger Pt particles [43,44], reducing the poisoning of the catalyst. At low current density ($< 0.1 \text{ A cm}^{-2}$) following ageing a decrease of the overpotential of the PEMFC with Pt/C as the anode catalyst can be observed in Figure 8, while the effect of RPC on the overpotential of the cells with Pt/GNS and Pt/N-GNP was negligible. Conversely for current density $> 0.15 \text{ A cm}^{-2}$, after RPC a decrease of the overpotential of the PEMFCs with Pt/GNS and, in particular, Pt/N-GNP as the anode catalysts were found, while the overpotential of the cell with Pt/C did not change.

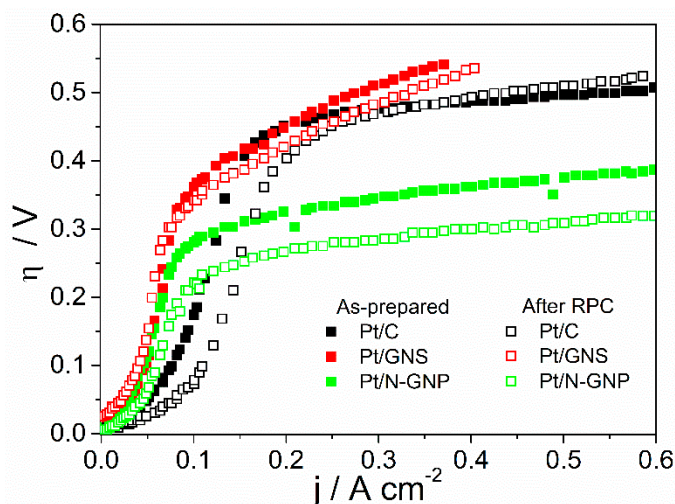


Figure 8. Overpotential vs. current density for Pt/C, Pt/GNS, and Pt/N-GNP catalysts before (closed symbols) and after (open symbols) RPC.

3. Materials and Methods

3.1. Catalyst Preparation

Graphene nanosheet (GNS) and nitrogen-doped graphene nanoplatelet (N-GNP) (both supplied by Graphene Supermarket®, Calverton, NY, USA)-supported platinum catalysts (20 wt % Pt) were prepared by the ethylene glycol (EG) method in alkaline medium (NaOH 0.1 mol L^{-1}). A $\text{H}_2\text{PtCl}_6 \cdot \text{H}_2\text{O}$ at 5% (Aldrich®, San Luis, MO, USA) solution was added and mixed with the carbon supports (Vulcan, GNS or N-GNP). Posteriorly this mixture was heated at 150°C , stirred, and was kept in argon atmosphere under reflux for 6 h. Afterward, the catalyst was neutralized with HCl 1.0 mol L^{-1} , dispersed into mili-Q® water, and centrifuged at 5000 rpm for 10 min, this process was repeated four times to assure the cleaning of the supported nanoparticles. Finally, the catalysts were filtered and after was kept for 1 h under hydrogen atmosphere at 200°C . Commercial carbon-supported platinum (Pt/C, 20 wt %) by Etek was used as anode catalyst (for comparison with Pt/GNS and Pt/N-GNP) and as cathode catalyst for all experiments.

3.2. Physical Characterization

The technique of X-ray Spectroscopy by Dispersive Energy (EDX) was used to obtain the mass ratio between carbon and Pt. The equipment used was a spectrometer (Zeiss-Leica® 440 Electron Microscopy Inc., Thornwood, NY, USA) with a SiLi detector. Thermogravimetric analyzes (TGA) were performed on the Mettler Toledo apparatus (Mettler Toledo, Columbus, OH, USA). The conditions used were: temperature range: $30\text{--}1000^\circ\text{C}$, using synthetic air as a gas at a heating rate of $10^\circ\text{C min}^{-1}$. The X-ray diffraction technique (XRD) was used to determine the structural characteristics of Pt-supported catalysts and to estimate the average sizes of the crystallites. The radiation used was $\text{CuK}\alpha$ ($\lambda = 0.15406 \text{ nm}$), generated at 40 kV and 30 mA, in a diffractometer (Rigaku®—ULTIMA IV, Akishima, Tokyo, Japan). The scans were obtained at 1° min^{-1} for 2θ between 10° and 100° . Using the Transmission Electronic Microscopy (TEM) technique, the average particle size, and distribution for each synthesized catalyst was determined, using a JEOL 2010 microscope (Akishima, Tokyo, Japan) with an energy of 200 keV and a filament of LaB_6 . X-ray Photon Spectroscopy (XPS, Thermo Scientific K-Alpha spectrometer®, Thermo Fischer Scientific, Waltham, MA, USA) using an incident photon energy of 1840 eV (Eph) from an InSb double crystal monochromator (111). The hemispheric electron analyzer was programmed to

pass electrons at an energy of 20 eV, with an energy pass of 0.2 eV and an acquisition time of 200 ms. The spectrum of each catalyst was obtained according to the elements that compose it.

3.3. Electrochemical Measurements

In order to test their electrochemical behavior, Pt/GNS, Pt/N-GNS, and Pt/C were used as anode catalysts and Pt/C (20 wt %) at the cathode, both with 0.4 mg Pt cm⁻², in a single PEMFC, as previously detailed in [27]. To perform the polarization curves, Fuel Cell Technologies work station equipment was utilized in the unit cell configuration (cell temperature: 85 °C) with H₂ and H₂/CO in the anode (100 mL min⁻¹, 2 atm and 100 °C), and O₂ in the cathode (150 mL min⁻¹, 1.70 atm and 90 °C). Before polarization measurements, the potential applied for 2 h was 0.7 V and 0.8 V for H₂ and H₂/CO respectively. The half-cell configuration was used for the Cyclic voltammetry (CV), CO stripping (SCO), and repetitive potential cyclic (RPC), and the work electrode was the anode with Ar and/or CO (for the SCO), in this case 20 min of CO followed by 40 min of Ar, the cathode was provided with H₂ employed as a reference electrode (RHE). The potential range was 0.075 to 0.9 V for CO stripping measurements. The potential range was 0.075 to 1.20 V at 20 mV s⁻¹ for CV tests and 0.075 to 0.70 V at 50 mV s⁻¹ for RPC used as the ageing test, applying 5000 cycles. The protocols used for CV, SCO, and RPC were detailed in Supplementary Materials.

4. Conclusions

The structural stability and the activity for hydrogen oxidation in the absence and in the presence of CO of pristine and nitrogen functionalized graphene-supported Pt electrocatalyst was utilized as anodes in PEMFCs. In the absence of N-functionalization, pristine graphene-supported Pt presents a higher structural stability but a lower CO tolerance than that of the carbon black-supported Pt. N-functionalization of graphene decreases its structural stability but remarkably improves its CO tolerance. The higher CO tolerance of Pt/N-GNP than that of Pt/GNS was ascribed to the presence of a defect in graphene, generated by N-doping, decreasing CO adsorption energy. The results of this experimental work, showing that the CO tolerance of graphene is strictly related to its functionalization, confirm the theoretical studies.

Supplementary Materials: The following are available online at <http://www.mdpi.com/2073-4344/10/6/597/s1>, The protocols used for CV, SCO, and RPC.

Author Contributions: Performed the experiments, M.G.-H.; methodology, M.G.-H., J.P.; data curation, M.G.-H., J.P., and E.A.; writing—original draft preparation, M.G.-H., J.P., and E.A. All authors have read and agreed to the published version of the manuscript.

Funding: This research was funded by São Paulo Research Foundation (FAPESP) (grant#2013/16930-7), CNPq (grant#313286/2018-3) and Coordenação de Aperfeiçoamento de Pessoal de Nível Superior—Brasil (CAPES)—Finance Code 1480786—Capes Proex.

Acknowledgments: LNNano for assisting with the XPS measurements (Project XPS-21416).

Conflicts of Interest: The authors declare no conflicts of interest.

References

1. Wee, J.-H.; Lee, K.-Y. Overview of the development of CO-tolerant anode electrocatalysts for proton-exchange membrane fuel cells. *J. Power Sources* **2006**, *157*, 128–135. [[CrossRef](#)]
2. Urian, R.C.; Gullá, A.F.; Mukerjee, S. Electrocatalysis of reformate tolerance in proton exchange membranes fuel cells: Part I. *J. Electroanal. Chem.* **2003**, *554–555*, 307–324. [[CrossRef](#)]
3. Narischat, N.; Takeguchi, T.; Mori, T.; Iwamura, S.; Ogino, I.; Mukai, S.R.; Ueda, W. Effect of the mesopores of carbon supports on the CO tolerance of Pt₂Ru₃ polymer electrolyte fuel cell anode catalyst. *Int. J. Hydrogen Energy* **2016**, *41*, 13697–13704. [[CrossRef](#)]

4. Ehteshami, S.M.M.; Chan, S.H. A review of electrocatalysts with enhanced CO tolerance and stability for polymer electrolyte membrane fuel cells. *Electrochim. Acta* **2013**, *93*, 334–345. [[CrossRef](#)]
5. Elezović, N.R.; Gajić-Krstajić, L.M.; Vračar, L.M.; Krstajić, N.V. Effect of chemisorbed CO on MoO_x-Pt/C electrode on the kinetics of hydrogen oxidation reaction. *Int. J. Hydrogen Energy* **2010**, *35*, 12878–12887. [[CrossRef](#)]
6. Gruver, G.A. The Corrosion of Carbon Black in Phosphoric Acid. *J. Electrochem. Soc.* **1978**, *125*, 1719. [[CrossRef](#)]
7. Kangasniemi, K.; Condit, D.A.; Jarvi, T. Characterization of Vulcan Electrochemically Oxidized under Simulated PEM Fuel Cell Conditions. *J. Electrochem. Soc.* **2004**, *151*. [[CrossRef](#)]
8. Maass, S.; Finsterwalder, F.; Frank, G.; Hartmann, R.; Merten, C. Carbon support oxidation in PEM fuel cell cathodes. *J. Power Sources* **2008**, *176*, 444–451. [[CrossRef](#)]
9. Antolini, E. Carbon supports for low-temperature fuel cell catalysts. *Appl. Catal. B Environ.* **2009**, *88*, 1–24. [[CrossRef](#)]
10. Antolini, E.; Gonzalez, E.R. Ceramic materials as supports for low-temperature fuel cell catalysts. *Solid State Ion.* **2009**, *180*, 746–763. [[CrossRef](#)]
11. Antolini, E.; Gonzalez, E.R. Polymer supports for low-temperature fuel cell catalysts. *Appl. Catal. A Gen.* **2009**, *365*, 1–19. [[CrossRef](#)]
12. Antolini, E. Graphene as a new carbon support for low-temperature fuel cell catalysts. *Appl. Catal. B Environ.* **2012**, *123*, 52–68. [[CrossRef](#)]
13. Heydari, A.; Gharibi, H. Fabrication of electrocatalyst based on nitrogen doped graphene as highly efficient and durable support for using in polymer electrolyte fuel cell. *J. Power Sources* **2016**, *325*, 808–815. [[CrossRef](#)]
14. Inagaki, M.; Toyoda, M.; Soneda, Y.; Morishita, T. Nitrogen-doped carbon materials. *Carbon* **2018**, *132*, 104–140. [[CrossRef](#)]
15. Groves, M.N.; Chan, A.S.W.; Malardier-Jugroot, C.; Jugroot, M. Improving platinum catalyst binding energy to graphene through nitrogen doping. *Chem. Phys. Lett.* **2009**, *481*, 214–219. [[CrossRef](#)]
16. Miao, H.; Li, S.; Wang, Z.; Sun, S.; Kuang, M.; Liu, Z.; Yuan, J. Enhancing the pyridinic N content of Nitrogen-doped graphene and improving its catalytic activity for oxygen reduction reaction. *Int. J. Hydrogen Energy* **2017**, *42*, 28298–28308. [[CrossRef](#)]
17. Tian, Y.; Liu, Y.-J.; Zhao, J.-X.; Ding, Y.-H. High stability and superior catalytic reactivity of nitrogen-doped graphene supporting Pt nanoparticles as a catalyst for the oxygen reduction reaction: A density functional theory study. *RSC Adv.* **2015**, *5*. [[CrossRef](#)]
18. Holme, T.; Zhou, Y.; Pasquarelli, R.; O'Hayre, R. First principles study of doped carbon supports for enhanced platinum catalysts. *Phys. Chem. Chem. Phys.* **2010**, *12*, 9461–9468. [[CrossRef](#)]
19. Liu, X.; Sui, Y.; Duan, T.; Meng, C.; Han, Y. Monodisperse Pt atoms anchored on N-doped graphene as efficient catalysts for CO oxidation: A first-principles investigation. *Catal. Sci. Technol.* **2015**, *5*, 1658–1667. [[CrossRef](#)]
20. He, D.; Jiang, Y.; Lv, H.; Pan, M.; Mu, S. Nitrogen-doped reduced graphene oxide supports for noble metal catalysts with greatly enhanced activity and stability. *Appl. Catal. B Environ.* **2013**, *132*, 379–388. [[CrossRef](#)]
21. Tang, Y.; Yang, Z.; Dai, X. A theoretical simulation on the catalytic oxidation of CO on Pt/graphene. *Phys. Chem. Chem. Phys.* **2012**, *14*, 16566–16572. [[CrossRef](#)] [[PubMed](#)]
22. Kim, G.; Jhi, S.-H. Carbon Monoxide-Tolerant Platinum Nanoparticle Catalysts on Defect-Engineered Graphene. *ACS Nano* **2011**, *5*, 805–810. [[CrossRef](#)] [[PubMed](#)]
23. Scardamaglia, M.; Bittencourt, C. Metal-free catalysis based on nitrogen-doped carbon nanomaterials: A photoelectron spectroscopy point of view. *Beilstein J. Nanotechnol.* **2018**, *9*, 2015–2031. [[CrossRef](#)] [[PubMed](#)]
24. Krishnan, R.; Su, W.-S.; Chen, H.-T. A new carbon allotrope: Penta-graphene as a metal-free catalyst for CO oxidation. *Carbon* **2017**, *114*, 465–472. [[CrossRef](#)]
25. Yoo, E.; Okata, T.; Akita, T.; Kohyama, M.; Nakamura, J.; Honma, I. Enhanced Electrocatalytic Activity of Pt Subnanoclusters on Graphene Nanosheet Surface. *Nano Lett.* **2009**, *9*, 2255–2259. [[CrossRef](#)]
26. Yoo, E.; Okada, T.; Akita, T.; Kohyama, M.; Honma, I.; Nakamura, J. Sub-nano-Pt cluster supported on graphene nanosheets for CO tolerant catalysts in polymer electrolyte fuel cells. *J. Power Sources* **2011**, *196*, 110–115. [[CrossRef](#)]

27. González-Hernández, M.; Antolini, E.; Perez, J. CO tolerance and stability of PtRu and PtRuMo electrocatalysts supported on N-doped graphene nanoplatelets for polymer electrolyte membrane fuel cells. *Int. J. Hydrogen Energy* **2019**, *45*, 5276–5284. [CrossRef]
28. Çögenli, M.S.; Bayrakçeken Yurtcan, A. Heteroatom doped 3D graphene aerogel supported catalysts for formic acid and methanol oxidation. *Int. J. Hydrogen Energy* **2020**, *45*, 650–666. [CrossRef]
29. Liu, C.-S.; Liu, X.-C.; Wang, G.-C.; Liang, R.-P.; Qiu, J.-D. Preparation of Nitrogen-Doped Graphene Supporting Pt Nanoparticles As a Catalyst for Oxygen Reduction and Methanol Oxidation. *J. Electroanal. Chem.* **2014**, *728*. [CrossRef]
30. Tao, L.; Dou, S.; Ma, Z.; Shen, A.; Wang, S. Simultaneous Pt deposition and nitrogen doping of graphene as efficient and durable electrocatalysts for methanol oxidation. *Int. J. Hydrogen Energy* **2015**, *40*, 14371–14377. [CrossRef]
31. Ma, J.-H.; Wang, L.; Mu, X.; Li, L. Nitrogen-doped graphene supported Pt nanoparticles with enhanced performance for methanol oxidation. *Int. J. Hydrogen Energy* **2015**, *40*, 2641–2647. [CrossRef]
32. Xin, Y.; Liu, J.-G.; Jie, X.; Liu, W.; Liu, F.; Yin, Y.; Gu, J.; Zou, Z. Preparation and electrochemical characterization of nitrogen doped graphene by microwave as supporting materials for fuel cell catalysts. *Electrochim. Acta* **2012**, *60*, 354–358. [CrossRef]
33. Avcioglu, G.S.; Ficicilar, B.; Bayrakceken, A.; Eroglu, I. High performance PEM fuel cell catalyst layers with hydrophobic channels. *Int. J. Hydrogen Energy* **2015**, *40*, 7720–7731. [CrossRef]
34. Chiang, Y.-C.; Liang, C.-C.; Chung, C.-P. Characterization of Platinum Nanoparticles Deposited on Functionalized Graphene Sheets. *Materials* **2015**, *8*, 6484–6497. [CrossRef] [PubMed]
35. Popova, A.N. Crystallographic analysis of graphite by X-Ray diffraction. *Coke Chem.* **2017**, *60*, 361–365. [CrossRef]
36. Saenko, N.S.; Ziatdinov, A.M. The small-angle γ -band of the X-ray diffraction for nanographite powder and its approximation by full-profile analysis. *Mater. Today Proc.* **2018**, *5*, 26052–26057. [CrossRef]
37. Leontyev, I.N.; Kuriganova, A.B.; Leontyev, N.G.; Hennes, L.; Rakhmatullin, A.; Smirnova, N.V.; Dmitriev, V. Size dependence of the lattice parameters of carbon supported platinum nanoparticles: X-ray diffraction analysis and theoretical considerations. *RSC Adv.* **2014**, *4*, 35959–35965. [CrossRef]
38. Naumov, O.; Naumov, S.; Abel, B.; Varga, A. The stability limits of highly active nitrogen doped carbon ORR nano-catalysts: A mechanistic study of degradation reactions. *Nanoscale* **2018**, *10*, 6724–6733. [CrossRef]
39. Chaban, V.; Prezhdo, O. Nitrogen-Nitrogen Bonds Violate Stability of N-Doped Graphene. *arXiv* **2015**, arXiv:1502.01939.
40. Arteaga, G.; Rivera-Gavidia, M.L.; Martínez, J.S.; Rizo, R.; Pastor, E.; García, G. Methanol Oxidation on Graphenic-Supported Platinum Catalysts. *Surfaces* **2019**, *2*, 16–31. [CrossRef]
41. Chandran, P.; Ghosh, A.; Ramaprabhu, S. High-performance Platinum-free oxygen reduction reaction and hydrogen oxidation reaction catalyst in polymer electrolyte membrane fuel cell. *Sci. Rep.* **2018**, *8*, 3591. [CrossRef] [PubMed]
42. Coros, M.; Varodi, C.; Pogacean, F.; Gal, E.; Pruneanu, M.S. Nitrogen-Doped Graphene: The Influence of Doping Level on the Charge-Transfer Resistance and Apparent Heterogeneous Electron Transfer Rate. *Sensors* **2020**, *20*, 1815. [CrossRef] [PubMed]
43. Gloaguen, F.; Le'Ger, J.M.; Lamy, C. Electrocatalytic oxidation of methanol on platinum nanoparticles electrodeposited onto porous carbon substrates. *J. Appl. Electrochem.* **1997**, *27*, 1052–1060. [CrossRef]
44. Bergamaski, K.; Pinheiro, A.L.N.; Teixeira-Neto, E.; Nart, F.C. Nanoparticle Size Effects on Methanol Electrochemical Oxidation on Carbon Supported Platinum Catalysts. *J. Phys. Chem. B* **2006**, *110*, 19271–19279. [CrossRef] [PubMed]

